Available online at www.sciencedirect.com
ScienceDirect
International Journal of Heat and Mass Transfer 50 (2007) 1314–1327
International Journal of HEAT and MASS TRANSFER
www.elsevier.com/locate/ijhmt

# Near-wall modeling of an isothermal vertical wall using one-dimensional turbulence

Harmanjeet Shihn, Paul E. DesJardin *

*Department of Mechanical and Aerospace Engineering, University at Buffalo, State University of New York, Buffalo, NY 14260-4400, USA*

Received 5 January 2006; received in revised form 15 September 2006
Available online 14 November 2006

**Abstract**

One-dimensional turbulence (ODT) modeling approaches are considered for describing the heat transfer from a vertical isothermal wall. In this approach, near wall gas-phase conduction processes are treated exactly while the effect of turbulent mixing is accounted for using triplet mapping stirring events. A new buoyancy generation production term is proposed, based on the vorticity transport scaling arguments, to account for the generation of large scale eddy mixing events. Both temporal and spatial implementations of ODT are explored and compared to the experimental data of Tsuji and Nagano. Comparisons of velocity, temperature, and Nusselt number show overall excellent agreement of simulation results to experimental data and to established inner and outer scaling laws for buoyancy driven boundary layers.


*Keywords:* Turbulent buoyancy driven boundary layers; One-dimensional turbulence; Near-wall modeling and scaling

## 1. Introduction

Turbulent boundary layers for vertically isothermal surfaces is important for many engineering applications and has been the subject of numerous investigations ranging from analytical theories of scaling behavior [1], to integral formulations [2], to detailed $k$–$\epsilon$ calculations [3,4] and most recently DNS and LES [5]. The challenge in modeling this class of flows is the coupling between the heat transfer at the wall surface and the generation of turbulence from buoyancy forces, which in turn, affect the temperature gradients and heat transfer at the wall. Predicting the heat transfer correctly at the wall is therefore critically important to accurately predict the overall flow evolution. Many previous near-wall models for RANS or LES make use of empirical near-wall modeling to estimate heat transfer via scaling theories that have had limited success for this category of flows. A more general approach to near-wall modeling is therefore desirable to allow for more complicated coupled molecular processes to be readily treated in a self-consistent manner.

One relatively recent advance in this area is the development of one-dimensional turbulence (ODT) modeling concepts of Kerstein [6,7]. In this approach, all molecular processes are explicitly resolved along a one-dimensional domain. A relatively coarse grid is however used in remaining orthogonal directions to greatly reduce computational cost. Turbulent mixing processes therefore cannot be explicitly resolved, but rather, are re-introduced along the one-dimensional domain using a model based on a prescribed stochastic process description. For the current application, the molecular processes consist of conduction and viscous stresses. Previous studies using ODT and its predecessor, the linear eddy model (LEM) [8] have shown to be successful at reproducing single-point statistical moments of flow variables when compared to DNS and experimental data for simple flows [6,9–12]. More recently, application of ODT to a buoyancy driven vertical slot [9]

* Corresponding author. Tel.: +1 716 645 2593x2314; fax: +1 716 645 3875.
*E-mail address:* ped3@buffalo.edu (P.E. DesJardin).

0017-9310/$ - see front matter © 2006 Elsevier Ltd. All rights reserved.
doi:10.1016/j.ijheatmasstransfer.2006.09.005

**Nomenclature**

| | |
|---|---|
| $A$ | ODT constant for shear, 0.5 |
| $B$ | ODT constant for buoyancy correction, 1.0 |
| $c_p$ | specific heat [kJ/kg K] |
| $g$ | acceleration due to gravity [m/s$^2$] |
| $Gr_y$ | local Grashoff number |
| $k$ | thermal conductivity [kW/m K] |
| $l$ | eddy length [m] |
| $L$ | length [m] |
| $Nu_y$ | local Nusselt number |
| $P_a$ | acceptance probability |
| $Pr$ | Prandtl number |
| $Re_T$ | eddy turbulence Reynolds number |
| $RMS$ | normalized root mean square, $(\sqrt{\bar{T}^2}/(\sqrt{\bar{T}^2})_{max})$, $(\sqrt{\bar{v}^2}/(\sqrt{\bar{v}^2})_{max})$ |
| $t$ | time [s] |
| $T$ | temperature [K] |
| $\bar{T}$ | time-averaged temperature [K] |
| $\bar{u}$ | time-averaged spanwise velocity [m/s] |
| $v$ | local streamwise velocity [m/s] |
| $\bar{v_b}$ | bulk velocity of 1D domain [m/s] |
| $\bar{v}$ | time-averaged streamwise velocity [m/s] |
| $x$ | distance from the wall [m] |
| $x_o$ | start location of eddy [m] |
| $y$ | distance from the leading edge of the wall [m] |
| $Z$ | ODT constant for viscous dissipation, 1.0 |

*Greek symbols*

| | |
|---|---|
| $\alpha$ | thermal diffusivity [m$^2$/s] |
| $\beta$ | volumetric coefficient of expansion, [K$^{-1}$] = $1/T_{avg}$ |
| $\delta_t$ | time step [s] |
| $\lambda_r$ | eddy rate distribution |
| $\nu$ | dynamic viscosity [m$^2$/s] |
| $\hat{\nu}$ | eddy mean viscosity |
| $\pi_t$ | Ruckenstein scaling parameter |
| $\rho$ | density [kg/m$^3$] |
| $\rho_o$ | reference density [kg/m$^3$] |
| $\theta$ | dimensionless temperature |
| $\tau$ | characteristic eddy time scale [s] |

*Subscripts and superscripts*

| | |
|---|---|
| avg | average |
| GC | George and Capp scaling |
| I | inner scaling variable |
| inf, $\infty$ | ambient |
| O | outer scaling variable |
| TN | Tsuji and Nagano scaling |
| w | wall |

shows good agreement to DNS results for mean temperature and velocity, as well as reproduces established Nusselt number scaling. The scaling behavior is especially remarkable since no explicit scaling behavior is assumed in the formulation, rather only local rules are enforced as to size and location of eddy events. LEM and ODT modeling also have shown similar success for application to reacting flows [13] and for use as a near-wall model for LES of convectively driven turbulent boundary layers [14].

The goal of the current study is to explore the use of ODT in this new setting for an isothermal vertical wall. Temporal and spatial ODT model descriptions are discussed with special emphasis on a new buoyancy production source term introduced for the turbulent eddy kinetic energy. Results are presented for mean temperature, velocity and Nusselt number with comparison to established scaling theory and experimental data of Tsuji and Nagano [15] and conclusions drawn for the applicability of ODT for this problem.

## 2. Problem statement

Fig. 1 shows a schematic of the vertical isothermal wall problem under consideration. Dirichlet boundaries are assumed for the wall temperature, $T_w = 333.15$ K, and far-field temperature, $T_\infty = 289.2$ K to match the experimental conditions of Tsuji and Nagano [15]. A no-slip boundary condition is imposed for the velocity at the wall and is assumed to approach zero in the far field. The temperature difference between the wall and ambient provides a buoyant force that drives the flow creating local mixing in the near-wall region. The initial velocity of the flow near the bottom of the wall is set equal to zero therefore the mean advection is determined solely from buoyancy forces. The relevant non-dimensional parameters

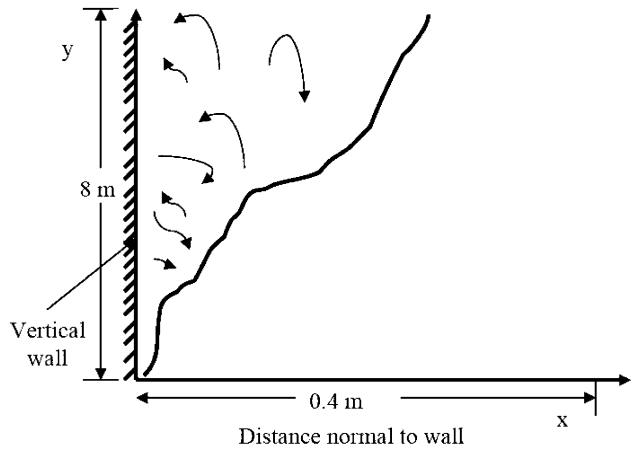


Fig. 1. Sketch of large scale-mixing event from baroclinic torque generated from a mismatch in hydrostatic pressure and density gradients.

defining the overall development of the flow are governed by the Grashoff, $Gr = g\beta(T_w - T_\infty)L^3/\nu^2$ and Prandtl, $Pr = \nu/\alpha$, numbers. The thermal diffusivity $\alpha$ and the dynamic viscosity $\nu$ are assumed to be constant and equal to $2.56 \times 10^{-5}$ and $1.59 \times 10^{-5}$ m$^2$/s, respectively, to match experimental conditions [15].

## 3. Modeling approach

The modeling approach for solution of the time-averaged flow-fields is based on the ODT modeling approach of Kerstein [6,7]. In this approach, the three-dimensional turbulence problem is reduced to a one dimensional representation. The advantage of this dimensional reduction is to allow for complete resolution of all molecular processes, thereby avoiding explicit modeling of higher order correlations that are required in moment based modeling approaches. The effects of turbulence mixing is treated using a series of random "triplet mapping" re-arrangement eddy events that serve to increase the local scalar gradients. An illustration of a triplet mapping event is shown in Fig. 2. During a mapping event, a segment of the flow field is first selected and the spatial extent reduced by a factor of three. Two additional copies are then created and the center copy mirror inverted resulting in a measure preserving re-arrangement event of the scalar field [6]. The location and frequency of these events are chosen based on a an instantaneous probability distribution function (PDF) which depends on local state of the flow-field.

The interpretation of the ODT domain is in general problem dependent. For the current study, the domain considered is oriented normal to the wall. Two implementation of ODT are explored. In the first, the ODT domain is regarded as a moving Lagrangian domain along the wall with a mean velocity, $\bar{v}_b$, as shown in Fig. 3. This interpretation allows for a correspondence between the simulation in time and the location of the ODT downstream and will referred to as the temporal implementation. In the second implementation, a collection of fixed ODT domains is considered forming a two-dimensional Cartesian grid as shown in Fig. 4. For this configuration, a parabolic formulation is pursued similar to that of Wei [16] and will referred to as the spatial implementation. In this approach a statistically stationary state is achieved to construct time-averaged properties and convection terms at subsequent downstream positions. Further details on each of these ODT implementations are discussed next.

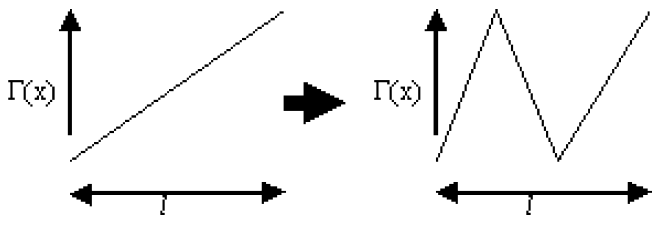


Fig. 2. Turbulent convective stirring from a single triplet-mapping stirring event.

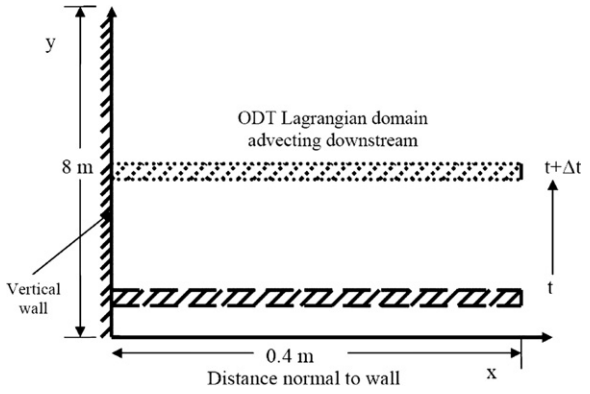


Fig. 3. Sketch of temporal ODT implementation for isothermal wall.

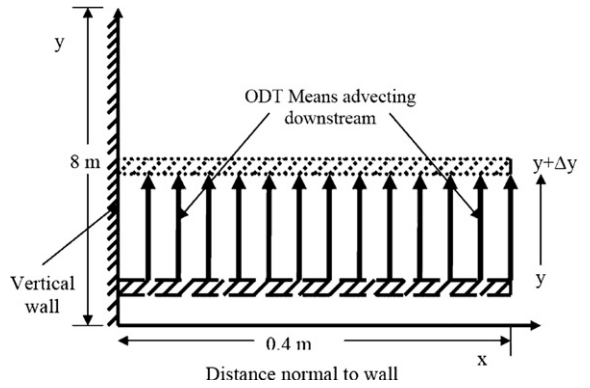


Fig. 4. Sketch of spatial ODT implementation for isothermal wall.

### 3.1. Temporal formulation

In the temporal formulation, the instantaneous transport equations governing the molecular processes in the ODT domain for streamwise momentum and temperature are solved on a moving domain.

$$\frac{\partial v}{\partial t} = \nu\frac{\partial^2 v}{\partial x^2} + g\beta(T - T_\infty), \tag{1a}$$

$$\frac{\partial T}{\partial t} = \alpha\frac{\partial^2 T}{\partial x^2}. \tag{1b}$$

In Eqs. (1a) and (1b) all transport properties are assumed constant and a Boussinesq approximation is used to relate changes in density to temperature resulting in the same set of equations as those used in the vertical cavity study of Dreeben and Kerstein [9]. The equations are integrated in time using standard Euler time advancement using second-order centered differences with Dirichlet boundary conditions for velocity and temperature. The spatial location of the moving ODT domain is determined by assuming the entire domain is advected at a bulk velocity, $\bar{v}_b$, defined as the ratio of the integrated momentum to mass fluxes similar to previous implementations of ODT [13]

$$\bar{v}_b(t) = \frac{\int_0^L \rho v^2(t)\mathrm{d}x}{\int_0^L \rho v(t)\mathrm{d}x}. \tag{2}$$

The bulk velocity is used to determine a corresponding downstream location, $y$, at a given time, $t$, in the ODT realization

$$y(t) = \int_0^t \bar{v}_b(t')\mathrm{d}t'. \tag{3}$$

Ensemble statistics are constructed from a sequence of Monte–Carlo realizations of the flow field and plotted as a function of downstream distance for comparison to experimental data.

### 3.2. Spatial formulation

The main limitation of the temporal formulation is the interpretation and definition of an appropriate bulk velocity given in Eq. (2). For flow configurations where the streamwise velocity varies little in the cross-stream direction, the exact definition is not critical. For boundary layers, however, this assumption may be limited therefore a spatial implementation is also pursued. In this case, a series of fixed ODT domains are arranged as shown in Fig. 4 in space for which time-averaged statistics are constructed. The time scales for updating the means is therefore larger compared to the time scales of the molecular diffusion and stirring events. The resolution between subsequent downstream ODT domains, $\Delta y$, is much larger than correlation length for which small scale mixing and molecular processes are correlated, therefore only time-averaged quantities are meaningful for exchange between the ODT domains. Exchanging instantaneous quantities by decreasing $\Delta y$ would effectively require DNS resolution thereby off-setting the advantages of using a one-dimensional approximation in the first place. The instantaneous equations for an ODT domain are expressed in a parabolized formulation resulting in the following continuity and the equations for the transport of velocity and temperature.

$$\frac{\partial \bar{u}}{\partial x} = -\frac{\partial \bar{v}}{\partial y}, \tag{4a}$$

$$\frac{\partial v}{\partial t} = -\left(\bar{u}\frac{\partial v}{\partial x}\right) - \left(\bar{v}\frac{\partial \bar{v}}{\partial y}\right) + \nu\frac{\partial^2 v}{\partial x^2} + g\beta(T - T_\infty), \tag{4b}$$

$$\frac{\partial T}{\partial t} = -\left(\bar{u}\frac{\partial T}{\partial x}\right) - \left(\bar{v}\frac{\partial \bar{T}}{\partial y}\right) + \alpha\frac{\partial^2 T}{\partial x^2}. \tag{4c}$$

The RHS of the equations has the same functional form as that for steady-state laminar natural convection. The quantities $\bar{u}$ and $\bar{v}$ are the time-averaged velocity at each ODT node that are constructed using an iterative time relaxation procedure at each downstream location. The continuity equation is then used to get $\bar{u}$ given converged value for $\bar{v}$. In this approach, the transport equations are numerically discretized as follows:

$$\phi_{i,j}^{n+1} = \phi_{i,j}^{n} - \delta t\left[\bar{v}_{i,j}\frac{\bar{\phi}_{i,j}^{*} - \bar{\phi}_{i,j-1}}{\Delta y}\right] + \frac{\Gamma\delta t}{\Delta x^2}\left(\phi_{i+1,j}^{n+1} - 2\phi_{i,j}^{n+1} + \phi_{i-1,j}^{n+1}\right) + S_\phi^n, \tag{5}$$

where $\Gamma = \nu$, $\alpha$ is the generalized transport coefficient and $\phi = v$, $T$ is a scalar that has a general advection, diffusion and source terms. The quantity $\bar{\phi}_{i,j-1}$ is time-averaged $\phi$ at the nearest upstream location. The value of $\bar{\phi}_{i,j}^{*}$ represents a tentative value of $\bar{\phi}_{i,j}$. To determine improved values of $\bar{\phi}_{i,j}$, Eq. (5) is first integrated in time using an implicit solver until a statistically stationary state of the flow is attained. Time-averages are then constructed to determine $\bar{\phi}_{i,j}$ which is then substituted back into Eq. (5) for $\bar{\phi}_{i,j}^{*}$. This process is repeated until the difference between $\bar{\phi}_{i,j}$ and $\bar{\phi}_{i,j}^{*}$ is smaller than a prescribed error tolerance – indicating a statistically converged state, i.e., $\bar{\phi}_{i,j}^{*} \to \bar{\phi}_{i,j}$.

## 4. ODT turbulent mixing

Turbulent mixing is modeled using a sequence of instantaneous triplet-mapping stirring events that represent the effects of turbulent eddies [6]. The mapping consists of the replacement of a 1D profile on the sampled segment with three identical copies compressed to one-third of their original length, with the middle copy mirror inverted as shown in Fig. 3. The result of an eddy event then maps the scalar $\phi(x) \to \phi(f(x))$, where $f$ is the mapping function with the following definition [6]:

$$f(x) \equiv x_o + \begin{cases} 3(x - x_o) & \text{if } x_o \leqslant x \leqslant x_o + l/3, \\ 2l - 3(x - x_o) & \text{if } x_o + l/3 \leqslant x \leqslant x_o + 2l/3, \\ 3(x - x_o) - 2l & \text{if } x_o + 2l/3 \leqslant x \leqslant x_o + l, \\ x - x_o & \text{otherwise,} \end{cases} \tag{6}$$

where $x_o$ is the starting point for the triplet map. The rate and location of the triplet mapping events are assumed to following a marked Poisson processes for which the probability that an eddy will take place of size, $l$, at location $x_o$, over time $\tau$ is equal to $\lambda(l,\tau)\,\mathrm{d}x_o\mathrm{d}l\mathrm{d}t$, where $\lambda$ is defined as the eddy rate distribution, defined as $\lambda = 1/l^2\tau$ [6]. Following earlier scalar implementations of ODT, the time scale, $\tau$, associated with eddy events is derived based on scaling arguments for the production/dissipation of eddy turbulent kinetic energy. Two mechanisms for eddy production are considered. The first is from velocity shear for which the rate of energy generation is assumed to be proportional to the local velocity shear.

$$\frac{l}{\tau} \sim \delta v, \tag{7}$$

where $\delta v$ is the velocity difference across the eddy. In more recent vector implementations of ODT, the generation of eddy kinetic energy can be more precisely defined in terms of the maximum available turbulent kinetic energy in the context of a modified mapping function that changes the amplitudes of the post-image velocity component, $v_I(f(y))$, to account for pressure scrambling [10], changes in potential energy [17] and compressibility effects [12]. In this study, simpler approach is pursued so as to include an additional mechanism for eddy production from baroclinic

torque generated from the mismatch in density and hydrostatic pressure gradients that is illustrated in Fig. 1. Guidance on estimating an eddy time scale for this event may be found by considering only the production term in the vorticity transport equation responsible for baroclinic torque

$$\frac{\mathrm{D}\vec{\omega}}{\mathrm{D}t} \sim \rho_\infty \frac{\nabla\rho \times \vec{g}}{\rho^2}. \tag{8}$$

Based on Eq. (8), a time scale for eddy production can be estimated for a given eddy

$$\frac{1}{\tau^2} \simeq \frac{1}{\bar{\rho}} g \frac{\delta\rho}{l}, \tag{9}$$

where $\bar{\rho}$ is the average density of the eddy and $\delta\rho$ similar to the velocity difference. Combining Eqs. (7) and (9) results in a balance equation for eddy turbulent kinetic energy

$$\underbrace{\left(\frac{l}{\tau(l;y,t)}\right)^2}_{\Delta KE} = \underbrace{(A\delta v)^2}_{\text{shear production}} + \underbrace{B\left(\frac{lg\delta\rho}{\rho_\mathrm{o}}\right)}_{\text{buoyancy production}} - \underbrace{Z\left(\frac{l}{\tau_\mathrm{d}}\right)^2}_{\text{vicous dissipation}} \tag{10}$$

The terms on the right-hand side of Eq. (10) represent the production of turbulent kinetic energy from shear and buoyancy forces and a sink term from viscous dissipation. The viscous dissipation term prohibits the formation of eddies that are smaller than viscous length scales where $\tau_\mathrm{d} = \frac{l^2}{16\hat{\nu}}$ is defined as a viscous time scale with $\hat{\nu} = \left(\frac{1}{l}\int_l^{x+l} \frac{\mathrm{d}s}{\nu(s)}\right)^{-1}$ [6]. The quantities $\delta v$ and $\delta\rho$ represent bulk differences in velocity and density across the eddy and are defined in terms of averages across the right and left sides of the eddy as

$$\delta v \text{ (or } \delta\rho) = \frac{2}{l}\left(\int_{x_\mathrm{o}}^{x_\mathrm{o}+(l/2)} v(x,t)(\text{or } \rho(x,t))\mathrm{d}x - \int_{x_\mathrm{o}+(l/2)}^{x_\mathrm{o}+l} v(x,t)(\text{or } \rho(x,t))\mathrm{d}x\right). \tag{11}$$

The second term on the RHS of Eq. (10) is to account for air engulfment from a long wave length instability modes. Using a Boussinesq approximation ($\delta\rho \simeq \bar{\rho}\beta\Delta T$), Eq. (10) is used to determine the mixing frequency, $\lambda$,

$$\lambda = \frac{1}{l^2\tau} = \frac{\nu}{l^4}\sqrt{A' Re_l^2 + B'\frac{\rho_\infty}{\bar{\rho}} Gr_l - Z'}, \tag{12}$$

where $Re_l (\equiv \delta v l/\nu)$ and $Gr_l (\equiv g\beta\Delta T\, l^3/\nu^2)$ are the eddy Reynolds and Grashoff numbers, and $A' = A^2$, $B' = B$ and $Z' = (16^2)Z$, where the constants are order unity and chosen to be $A = 0.5$, $B = 1.0$ and $Z = 1.0$ in this study, consistent with previous ODT implementations. As will be discussed in the results, the predictions are fairly insensitive to the exact choice of these constants.

As discussed by Kerstein [6], the probability density given in Eq. (12) can in principle be sampled by first constructing the distribution for all possible values of $l$ and $x_\mathrm{o}$ and then sampling from that distribution [6]. The cost of implementing such an approach however is prohibitive and therefore a generalized rejection method is pursued as discussed in [6]. Further discussion of this approach will be discussed in the results.

The eddy selection procedure however may occasionally result in the occurrence of unphysical large eddies that will dominate the overall scalar evolution. To remedy this issue, a large scale eddy suppression mechanism is introduced. For this study, the median model is implemented for which a linear profile across the eddy range is first constructed with a slope corresponding to the median of $|\mathrm{d}v/\mathrm{d}x|$ across the eddy range. This velocity gradient is used to determine a minimum reference eddy rate probability, $\lambda_{\min}$. If $\lambda_{\text{assumed}} < \lambda_{\min}$ then the selected eddy is rejected [6].

## 5. Results and discussion

Comparisons of ODT predictions to the theory and experiment of Tsuji and Nagano for an isothermal wall are made in this study. In the experiment a copper plate measuring 4 m high and 1 m wide is at a uniform temperature of 333.15 K in an ambient atmosphere at 289.2 K. Two V-shaped hot wires and a cold wire were used to measure the temperature and velocity of the flow field at several downstream locations [15]. In both the temporal and spatial ODT implementations, a total of 800 grid points are used in the wall normal direction producing a 0.5 mm resolution. For the spatial formulation, a coarser grid of 1 cm resolution is employed in the streamwise direction to resolve only mean flow quantities. For the temporal formulation, a total of 1000 realizations are collected to construct mean and RMS statistics as a function of time. These quantities are then plotted as a function of downstream distance using Eq. (3).

### 5.1. Comparison to theory and experimental data

Fig. 5 shows contour plots of (a) temperature and (b) streamwise velocity for a single ODT realization using the temporal formulation. As the flow accelerates downstream, progressively larger eddy stirring events are observed resulting in the engulfment of surrounding air. Ensemble average contour plots of temperature and velocity are shown in Fig. 6 with detailed profiles summarized in Fig. 7 at downstream locations of $x = 2$, 4, 6 and 8 m. The local velocity maximum occurs very near the wall from a balance of local buoyancy forces and the viscous shear stress from the no-slip boundary condition at the wall. The boundary layer of buoyancy driven flows is therefore very different from convectively driven boundary layers where the velocity maximum occurs in the free-stream. In terms of the inner scaling, the principle difference is that the sum of the viscous $(-\mu\partial\bar{v}/\partial x)$ and turbulent $(-\overline{u'v'})$ shear stresses are constant across the boundary layer thickness for convectively driven boundary layers, while this is not the case for buoyancy driven boundary layers. In the

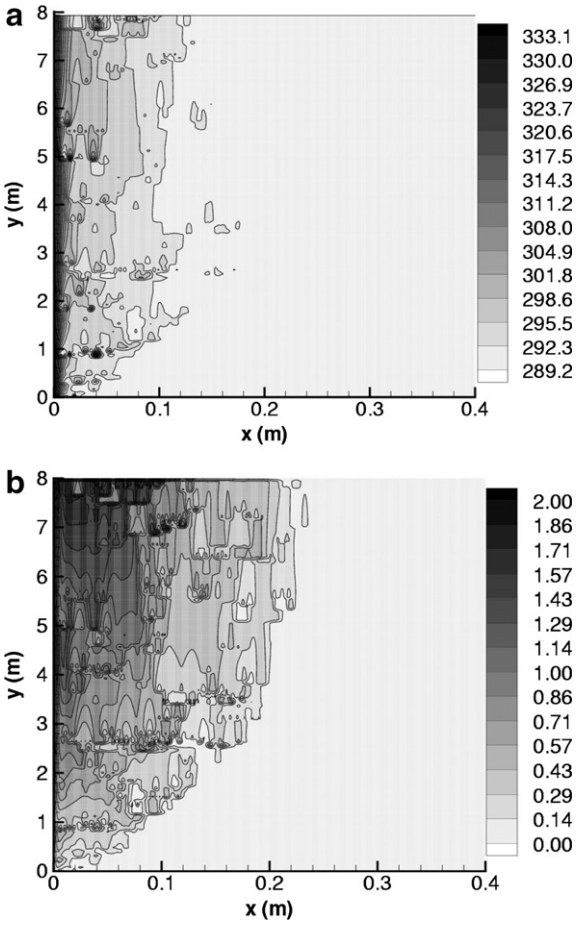


Fig. 5. Instantaneous snapshots of (a) temperature (K) and (b) streamwise velocity (m/s) from a single ODT realization using the temporal formulation.

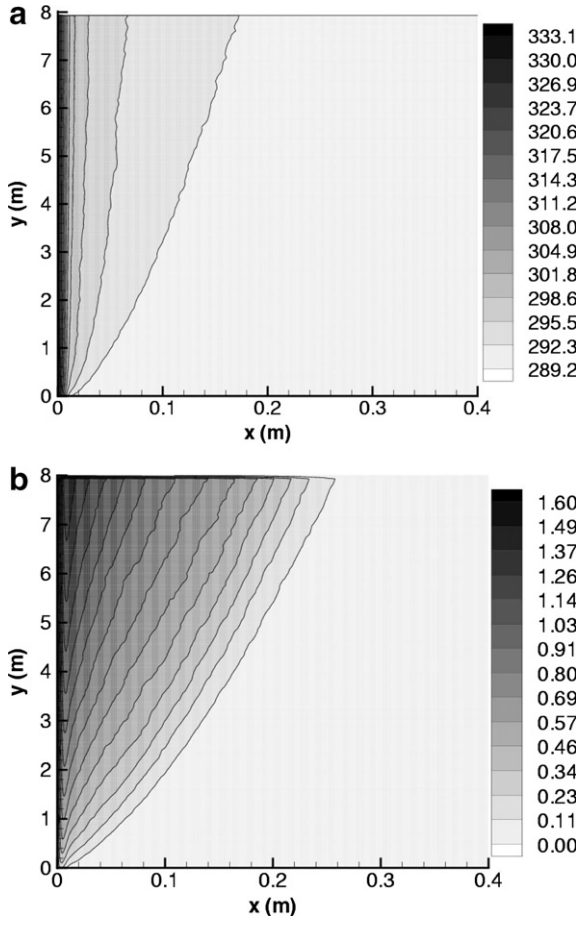


Fig. 6. Ensemble average (a) temperature (K) and (b) streamwise velocity (m/s) contours using the temporal formulation.

latter case, the sum of the conduction, $-k\partial\bar{T}/\partial x$, and turbulent flux, $-\overline{u'T'}$, is constant in the near-boundary region and equal to the total near-wall heat flux, $q_w$. Using this observation, George and Capp (GC) developed inner scaling relations for the temperature ($(\bar{T}-T_w)/T_I$) and velocity ($\overline{v}/v_I$) profiles assuming the near-wall temperature and velocities depend solely on $g\beta$, $q_w$ and $k$ [1],

$$L_I^{GC} = \left(\frac{\alpha^3}{g\beta F_o}\right)^{1/4}, \tag{13a}$$

$$T_I^{GC} = F_o^{3/4}(g\beta\alpha)^{-1/4}, \tag{13b}$$

$$v_I^{GC} = (g\beta F_o\alpha)^{1/4}, \tag{13c}$$

where $L_I$, $T_I$ and $v_I$ are the inner scalings for length, temperature and velocity, respectively. GC also developed outer layer scaling relations where it is assumed that molecular processes are negligible at sufficiently far distances from the wall. These scaling are expressed in terms of velocity ($\overline{v}/v_o$) and temperature ($(\bar{T}-T_w)/T_O$) deficit profiles assuming that they are functions of $q_w$, $g\beta$ and an outer scaling length, $L_O^{GC}$, that is assumed to be equal to momentum thickness, $\delta_v$.

$$L_O^{GC} = \delta_v, \tag{14a}$$

$$T_O^{GC} = q_w^{2/3}(g\beta\delta)^{-1/3}, \tag{14b}$$

$$v_O^{GC} = (g\beta q_w\delta k)^{1/4}. \tag{14c}$$

Figs. 8 and 9 show mean temperature and velocity profiles using the inner and outer scaling proposed by GC, respectively. The temperature profiles are observed to collapse nicely, consistent with the theory. The velocity profiles, however, show only a limited range of collapse for $x/L_I^{GC} < 1$ and $x/L_O^{GC} > 1.5$ for the inner and outer ranges, respectively. These trends are consistent with that observed by Dreeben and Kerstein for ODT and DNS predictions of a vertical isothermal channel [9]. The reason for the lack of collapse for velocity may be attributed to two possible reasons. The first is the relatively low values of $Gr_y$ considered. For low values of $Gr_y$, a distinct scale separation between inner and outer flow dynamics may not exist therefore the arguments for these distinct regions no longer hold true. The second reason is that the scaling estimates of GC are only strictly valid for constant heat flux boundary conditions, therefore may have some limited applicability for the current isothermal wall case.

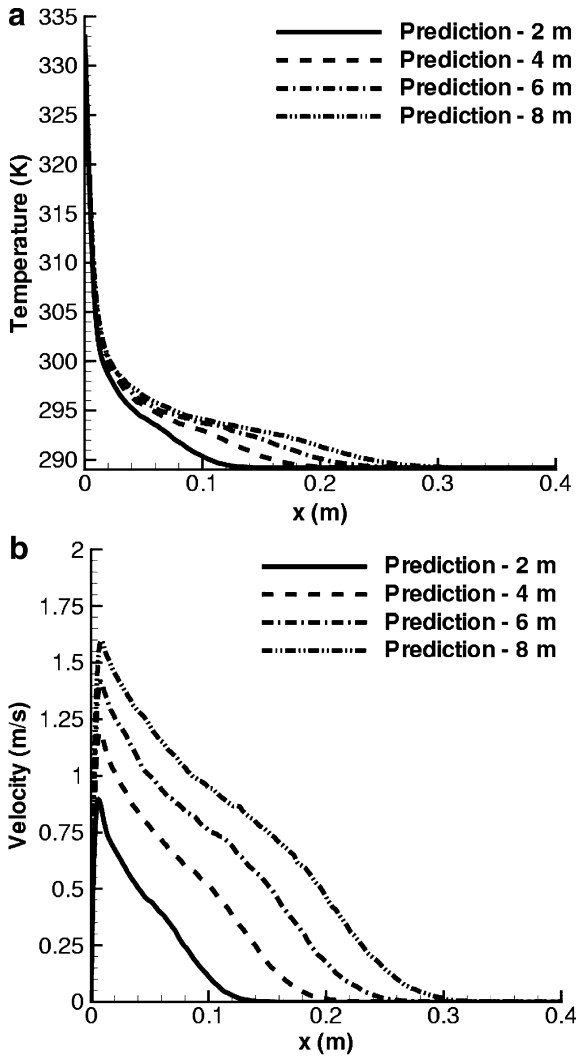


Fig. 7. Ensemble average (a) temperature (K) and (b) stream-wise velocity (m/s) profiles at $x = 2$, 4, 6 and 8 m downstream using the temporal formulation.

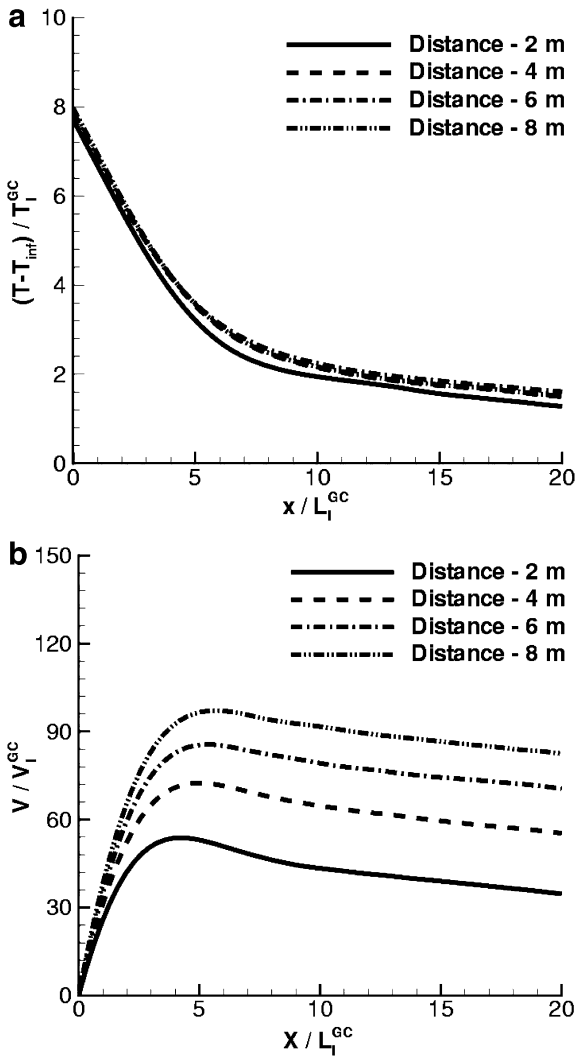


Fig. 8. Ensemble average (a) temperature and (b) streamwise velocity profiles at $x = 2$, 4, 6 and 8 m downstream using inner variable scaling of George and Capp [1].

Alternatively, Tsuji and Nagano (TN) considered scaling of the inner layer using similarity variables for a laminar boundary layer flow, $L_{\mathrm{IV}}^{\mathrm{TN}} = (x/y)Gr_y^{1/4}$, and show excellent collapse of inner mean and RMS velocity [15]. For the temperature, they suggest correlating the inner temperature profiles using the heat flux, or more precisely, a non-dimensional heat flux at the surface, $L_{\mathrm{IT}}^{\mathrm{TN}} = -x(\partial\theta/\partial x)|_{x=0}$, where $\theta = (\bar{T} - T_{\mathrm{w}})/(T_{\mathrm{w}} - T_{\infty})$. Similar arguments are used for the normalization of the velocity and temperature resulting in the following set of inner scaling variables:

$$L_{\mathrm{IV}}^{\mathrm{TN}} = (1/y)Gr_y^{1/4}, \tag{15a}$$

$$L_{\mathrm{IT}}^{\mathrm{TN}} = -(\partial\theta/\partial x)|_{x=0}, \tag{15b}$$

$$T_{\mathrm{I}}^{\mathrm{TN}} = T_{\mathrm{w}} - T_{\infty}, \tag{15c}$$

$$v_{\mathrm{I}}^{\mathrm{TN}} = Gr_y^{1/2}v/y. \tag{15d}$$

For the outer scaling TN found that their data collapses if the distances are scaled by the thermal and momentum boundary layer thicknesses resulting in the following set of outer scalings:

$$L_{\mathrm{OV}}^{\mathrm{TN}} = \delta_{\mathrm{v}}, \tag{16a}$$

$$L_{\mathrm{OT}}^{\mathrm{TN}} = \delta_{\mathrm{T}}, \tag{16b}$$

$$T_{\mathrm{O}}^{\mathrm{TN}} = T_{\mathrm{w}} - T_{\infty}, \tag{16c}$$

$$v_{\mathrm{O}}^{\mathrm{TN}} = v_{\max}, \tag{16d}$$

where $\delta_{\mathrm{T}}$ and $\delta_{\mathrm{v}}$ are the integral thermal or momentum boundary layer thicknesses defined as $\delta_{\mathrm{T}} = \int_0^L \theta(x)\mathrm{d}x$ and $\delta_{\mathrm{v}} = \int_0^L (v(x)/v_{\max})\mathrm{d}x$, respectively. Comparison of ODT predictions of normalized boundary layer thicknesses are shown in Fig. 10 with comparison to the experimentally obtained empirical relations from TN (Fig. 11)

$$U_{\mathrm{b}}\delta_{\mathrm{v}}/v = 0.331Gr_y^{0.250}, \tag{17a}$$

$$U_{\mathrm{b}}\delta_{\mathrm{T}}/v = 0.646Gr_y^{0.151}, \tag{17b}$$

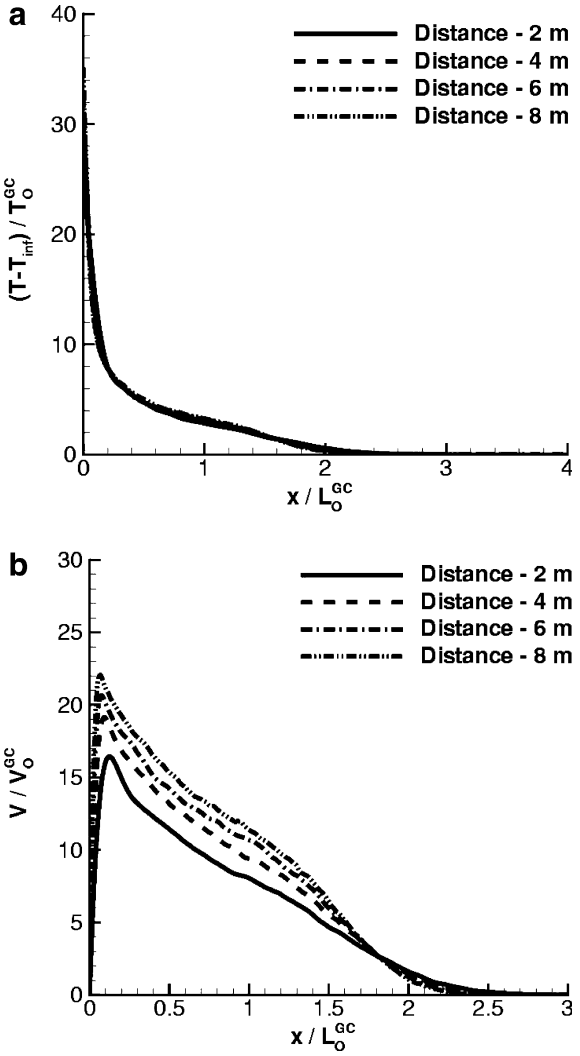


Fig. 9. Ensemble average (a) temperature and (b) streamwise velocity profiles at $x = 2$, 4, 6 and 8 m downstream using outer variable scaling of George and Capp [1].

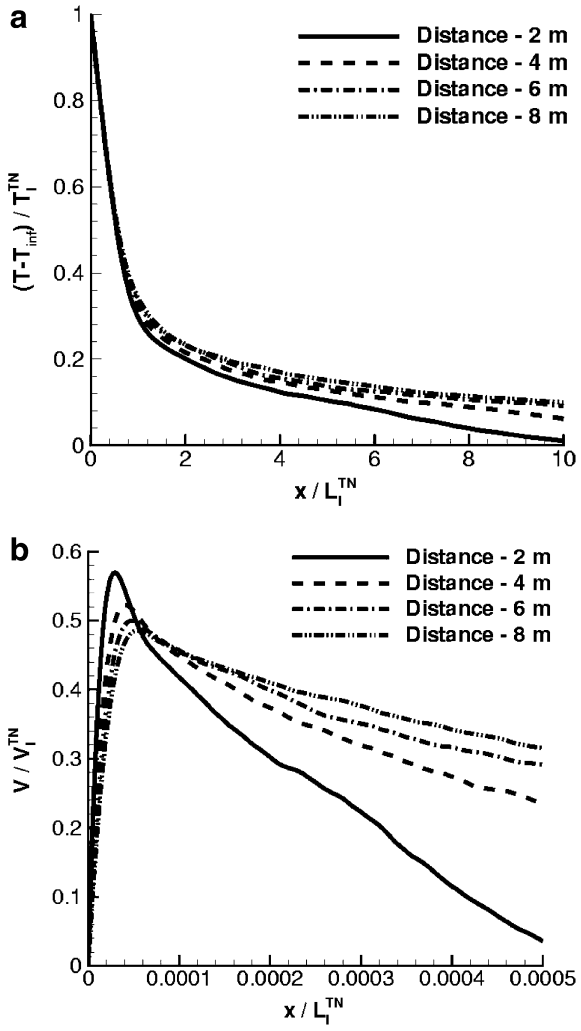


Fig. 11. Ensemble average (a) temperature and (b) streamwise velocity profiles at $x = 2$, 4, 6 and 8 m downstream using inner variable scaling of Tsuji and Nagano [15].

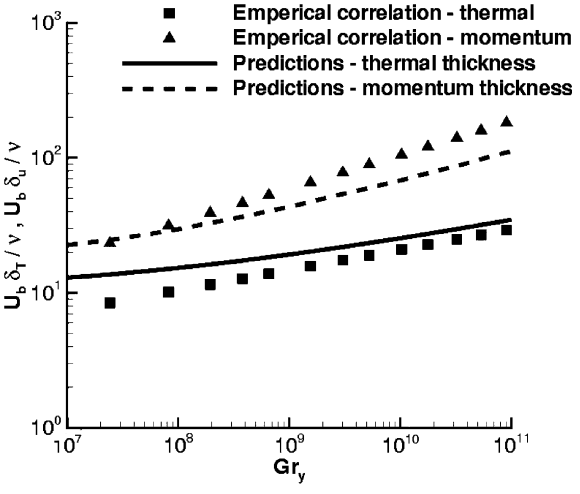


Fig. 10. Normalized thermal ($U_b\delta_T/\nu$) and momentum ($U_b\delta_U/\nu$) boundary layer thicknesses vs. $Gr_y$ ($=g\beta(T_w - T_\infty)y^3/\nu^2$).

where $U_b(=(g\beta(T_w - T_\infty)\nu)^{1/3})$ is a reference velocity. As expected, the momentum boundary layer thickness grows faster than the thermal boundary layer thickness for the $Pr < 1$ case considered. The overall agreement of the predictions to the experimentally derived empirical correlations is good.

Comparisons of velocity and temperature profiles using the outer scaling suggested by TN with comparison to their data are presented in Fig. 12 for (a) temperature and (b) velocity at several downstream locations. The profiles collapse between 6 and 8 m downstream indicating a self-similar state. Overall agreement with the experimental data are excellent with maximum errors of 3% and 15% for the temperature and velocity, respectively. Also included in the profile comparisons in the result from the spatial formulation at $y = 8$ m downstream. Overall, predictions for temperature using the spatial formulation are almost identical to the temporal formulation. Predictions of stream-wise velocity show the spatial formulation slightly

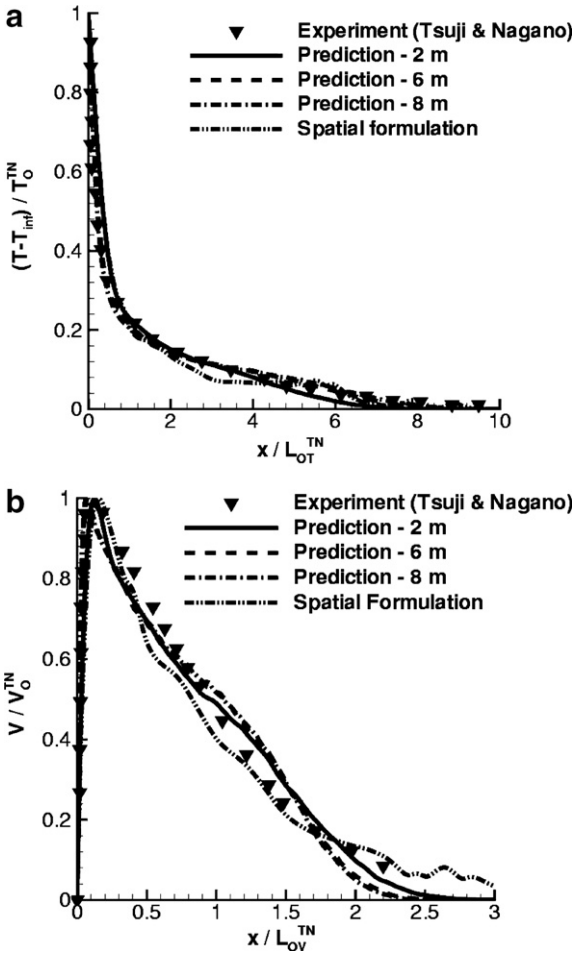


Fig. 12. Ensemble average (a) temperature and (b) streamwise velocity profiles at $x = 2$, 4 and 8 m downstream along with the solution for spatial formulation using outer variable scaling of Tsuji and Nagano [15].

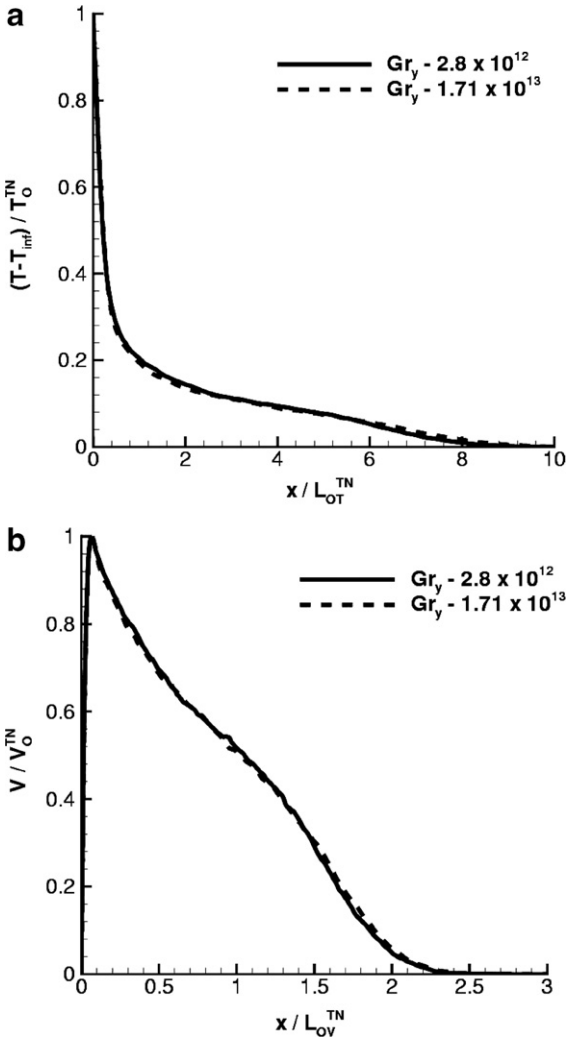


Fig. 13. Ensemble average (a) temperature and (b) streamwise velocity profiles for increasing *Gr* using outer variable scaling of Tsuji and Nagano [15].

under-predicts the streamwise velocity with maximum error of 16% but is able to predict the far-field entrainment velocity slightly better than the temporal formulation. To further examine the general applicability of these scaling relations, the temperature difference between the wall and the far-field is increased by a factor of 10 resulting in a factor of 6.1 increase in the Grashoff number. Fig. 13 shows a comparison of this case with the baseline case at $y = 8$ m. No differences are observed, suggesting that the outer scalings from TN are very reasonable.

Fig. 14 shows comparisons of normalized temperature and velocity RMS profiles using the TN outer scaling with comparison to their data. The local peak in velocity observed in Fig. 12(b) results in the narrow RMS velocity profile compared to that for temperature. For a turbulent kinetic energy production standpoint, the peak in velocity provides two regions of shear and therefore an increase in TKE production. In contrast, the average temperature monotonically decreases from the wall to the far-field temperature resulting in a more distributed region of temperature variance. Qualitatively the ODT predictions are in

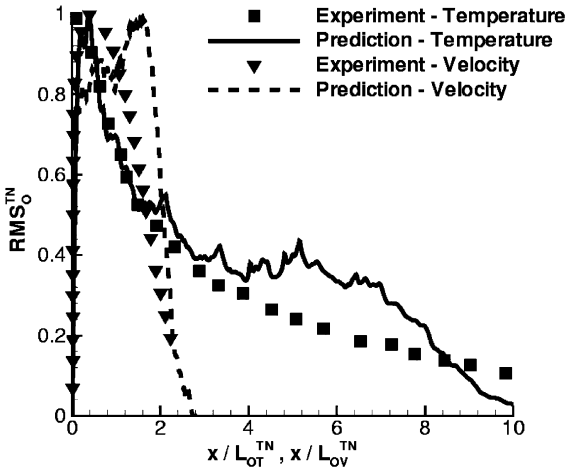


Fig. 14. Normalized RMS of temperature and velocity using temporal formation at self-similar state.

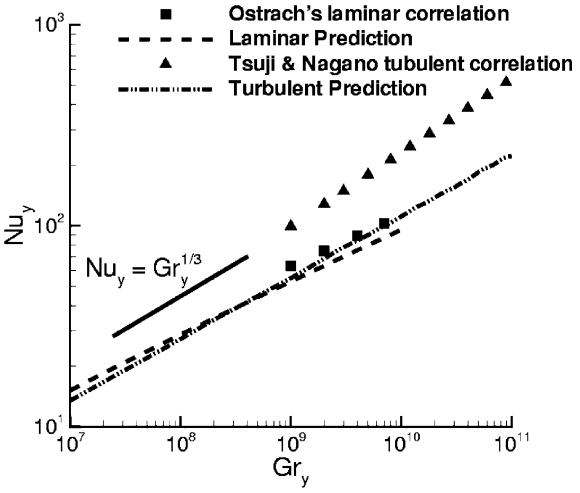


Fig. 15. Predictions of $Nu$ vs. $Gr_y$ compared to laminar boundary layer theory, $Nu_y = 0.355Gr_y^{1/4}$ [18] and experimental data, $Nu_y = 0.11Gr_y^{1/3}$, of Tsuji and Nagano [15].

good agreement to the data with respect to the extent of the distributions. However, two local maxima are predicted using ODT rather than just one maxima observed in the data. The two local maxima in the RMS is consistent with previous ODT simulations and is attributed to an artifact associated with the implementation of the triplet-mapping event near the wall [14].

Fig. 15 present comparisons of $Nu_y(=hy/k)$ number vs. $Gr_y(=g\beta(T_w - T_\infty)y^3/v^2)$ number both with and without (laminar case) the ODT stirring mechanism. For the case without stirring, predictions of $Nu_y$ compare very well to the laminar boundary layer correlation of Ostrach, $Nu_y = 0.355Gr_y^{1/4}$ [18]. Cases with stirring activated agree well to the experimental correlation of TN, $Nu_y = 0.11Gr_y^{1/3}$, with a scaling behavior following a 1/3 power law. Quantitatively, however, the prediction of $Nu_y$ appears to be a factor of two low. This result is consistent with previous ODT studies of flow in a vertical channel for which the $Nu$ was also a factor of two lower with comparison to DNS [9]. A possible reason for the observed differences may be in part the ambiguity in defining the downstream spatial location using the bulk velocity (Eq. (3)) using the temporal formulation. To remove this uncertainty, cases are also conducted using the spatial formulation, however, the results are almost identical to those based on the temporal formulation.

More generally, $Nu_y$ is well known to be a function of both $Gr_y$ and the $Pr$ number for which empirically based correlations are available [19]. Fig. 16(a) shows ODT cases with the $Pr$ increased and decreased by a factor of 10. Increasing the $Pr$ decreases the thermal boundary layer thickness, $\delta_T$, and increases the local heat transfer. Recently, Ruckenstein developed a heat transfer correlation applicable over a wide range of Prandtl numbers by proposing an interpolation expression for $Nu_y$ and using

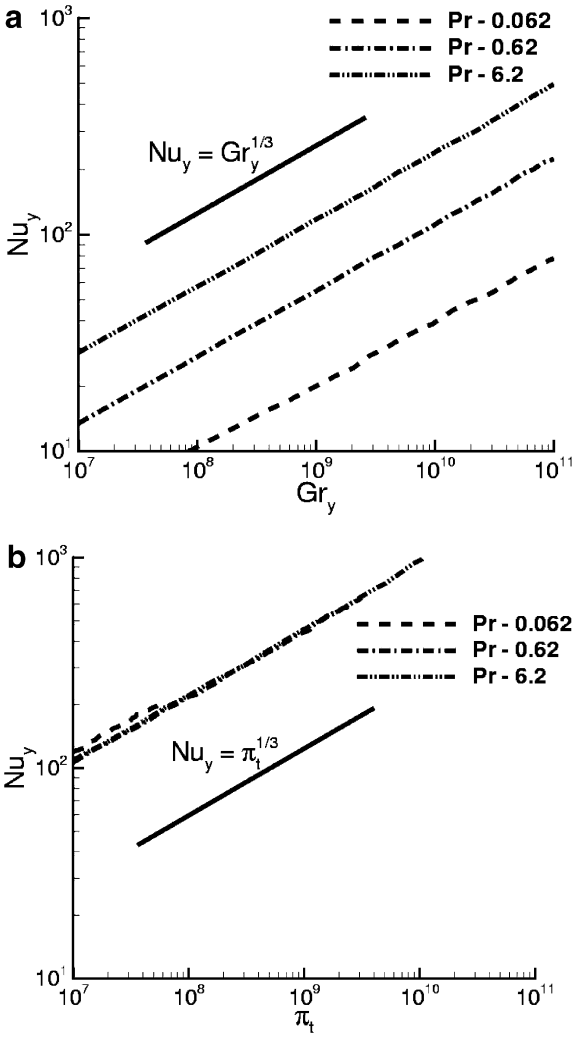


Fig. 16. Predictions of $Nu_y$ sensitivity to $Pr$ number as a function of (a) $Gr_y$ and (b) $\Pi_t = Gr_yPr^2(41.96 + 58.43Pr)^{-4/3}$ [20].

the limiting cases of $Pr \to \infty$ and $Pr \to 0$ to solve for two unknown constants, resulting in the following expression [20,21]:

$$Nu_y = Gr_y^{1/3}Pr^{2/3}(C_1 + C_2Pr)^{-4/9}, \tag{18}$$

where $C_1 = 41.96$ and $C_2 = 58.43$. Ruckenstein further suggested that Eq. (18) can also be expressed in terms of a single non-dimensional grouping, $Nu_y = \pi_t^{1/3}$, where $\pi_t = Gr_yPr^2(C_1 + C_2Pr)^{-4/3}$. Fig. 16(b) shows the result from Fig. 16(a) expressed in terms of $\pi_t$. As shown, the ODT predictions of $Nu_y$ collapse to a single curve in excellent agreement with the theory.

### 5.2. ODT model sensitivity

#### 5.2.1. Model constants

Figs. 17–19 summarize the sensitivity of the results to the model constants $A$, $B$ and $Z$. Additional

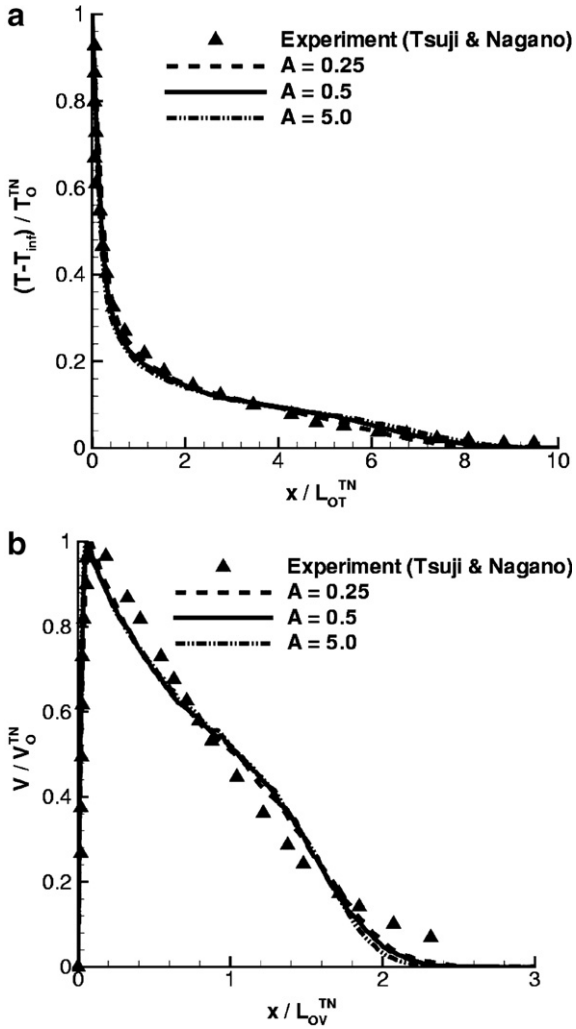


Fig. 17. Sensitivity of normalized mean (a) temperature and (b) velocity predictions to model constant $A$.

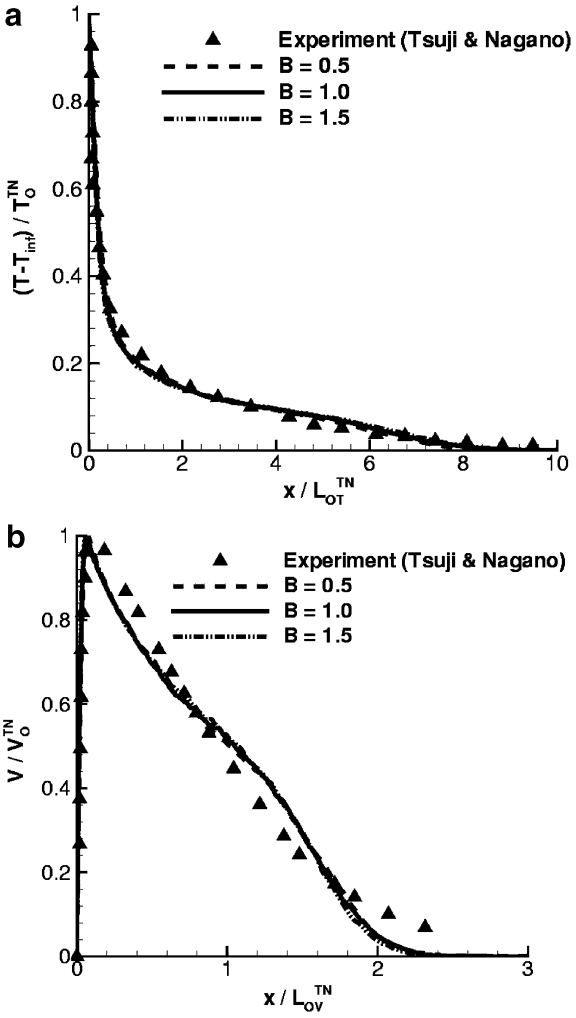


Fig. 18. Sensitivity of normalized mean (a) temperature and (b) velocity predictions to model constant $B$.

simulations are conducted with variations of each of these constants by ±50% for $A$ and $B$, and ±100% for $Z$. Constants $A$ and $B$ are the proportionality factors which account for the dependency of eddy production from velocity shear and density gradients, respectively. Figs. 17 and 18 show that varying $A$ or $B$ by 50% results in more mixing in the outer layer consistent with the physical interpretation of the constants. However, the maximum difference in mean temperature and streamwise velocity from the baseline case is only 3% and 5%, respectively, showing the robustness of the modeling approach.

Fig. 19 shows the sensitivity of mean temperature and velocity with variations in $Z$ by ±100%. As shown, almost no difference in the overall profiles is observed. The reason for this is that the mean profiles are dominated by the large eddy turnover events. The constant $Z$ controls the extent of small scale eddy suppression and therefore has little affect on the larger scales of motion, consistent with classical theories of turbulence.

### 5.2.2. Numerical parameters

As discussed in Section 4, the probability density given in Eq. (12) can in principle be sampled by first constructing the distribution for all possible values of $l$ and $x_o$ and then sample it [6]. The cost of implementing such an approach however is prohibitive and therefore a generalized rejection method is pursued as discussed in [6] In this case, a trial joint PDF for eddy size and location is first assumed that has the functional form, $\lambda_{\text{assumed}} = f(l)g(x_o)$, where $f(l)$ and $g(x_o)$ defined the probability density for the size and location, respectively [6]. The rejection method is implemented by first sampling from $f(l)$ and $g(x_o)$ to determine the size and location of a trial eddy. Once an trial eddy is selected then an acceptance probability $P_a = \lambda/\lambda_{\text{assumed}} = \lambda\Delta t_{\text{stir}}/(f(l)g(x_o))$, is determined and a separate random number, RN, is sampled. If RN is less than $P_a$ then the eddy is implemented, otherwise the eddy is rejected. This approach to implementing eddy events can be thought of a more generalized rejection approach to sampling a given PDF [22,23]. In this study,

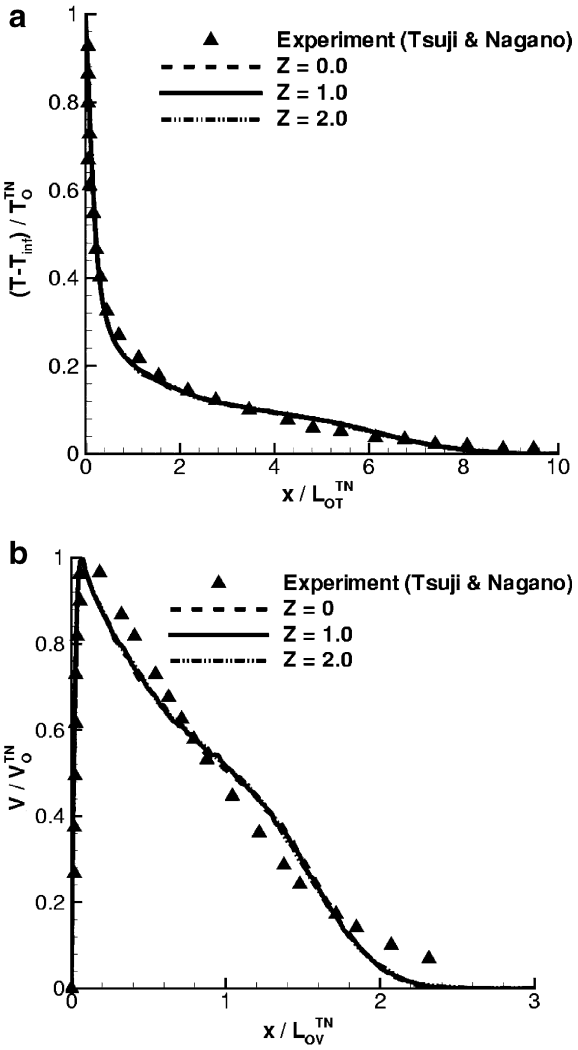


Fig. 19. Sensitivity of normalized mean (a) temperature and (b) velocity predictions to model constant $Z$.

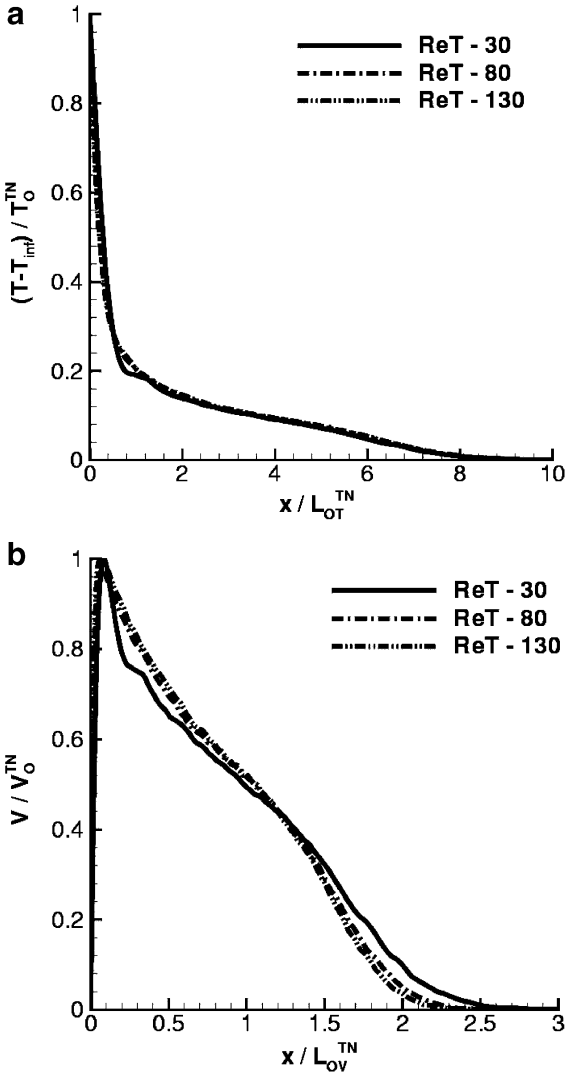


Fig. 20. Sensitivity of normalized mean (a) temperature and (b) velocity predictions to $Re_T$ used in ODT rejection sampling method.

the linear eddy model (LEM) is employed as the trial PDF,

$$f(l) = \frac{3-p}{L[Re_T^{3/p-1} - 1]} \left(\frac{l}{L}\right)^{p-4} \tag{19}$$

and is parameterized by an integral length scale of turbulence, $L_k$, a turbulence Reynolds number, $Re_T$, and a high Reynolds number scaling parameter, $p(=4/3)$. The most important issues for selecting these parameters is to ensure that the trial PDF spans the size range of all possible eddy events. To guarantee this to be the case, the $L_k$ is chosen to be the entire domain width and $Re_T$ is increased until the results are independent of this parameter. Increasing $Re_T$ increases the range of possible eddy sizes. For a fixed $L_k$, this forces the selection of smaller eddies. A disadvantage of selecting a $Re_T$ too large will be the added CPU cost of excessive sampling to obtain enough realization construct ensemble statistics. Fig. 20 shows normalized (a) temperature and (b) velocity results with $Re_T$ chosen as 30, 80 (baseline) and 130. As shown, results using $Re_T = 80$ and 130 are nearly identical indicating that the results are independent for $Re_T \geqslant 80$. In contrast, for $Re_T = 30$ the results are not correct since at this low Reynolds number the range of possible eddy sizes is artificially limited to relatively large eddies.

Another consideration in the formulation of the ODT model for boundary layer flows is the size of the computational domain. At the free right boundary, the velocity is assumed equal to zero and the temperature equal to the far-field temperature. These boundary conditions are valid as long as the domain is chosen to be sufficiently large. To observe the effects of the ODT domain size and to make sure that the solution is independent of it, two different domain sizes were advected downstream, with the bulk velocity as mentioned before. Fig. 21 show comparisons of (a) temperature and (b) velocity profiles using the baseline 0.4 m and doubling the domain size to 0.8 m. As shown, the results are almost identical, indicating that the 0.4 m is a sufficiently large domain.

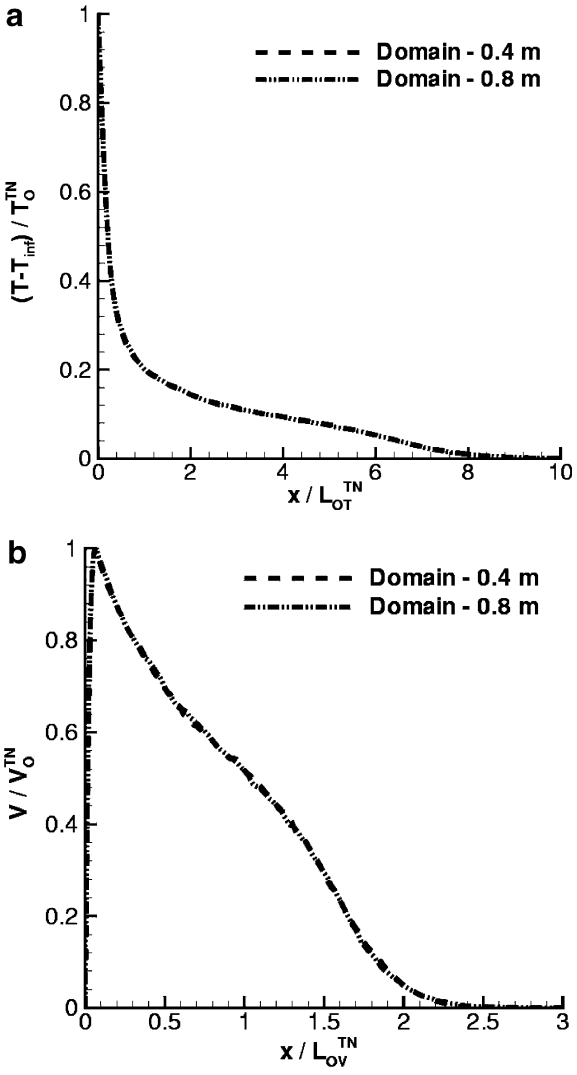


Fig. 21. Sensitivity of normalized mean (a) temperature and (b) velocity predictions to domain size.

## 6. Conclusions

In this study, temporal and spatial stand-alone ODT models are developed for modeling vertical buoyancy driven turbulent boundary layers for an isothermal wall. In this formulation, an eddy generation term is introduced that accounts for the generation of long wavelength instability modes. This term is formulated based on time-scales estimated from the buoyancy source term that arises in the vorticity transport equation. Overall, excellent agreement is observed between ODT predictions and the experimental data for time-averaged mean velocity and temperature. Differences however are observed for the RMS comparisons. Two local maxima are predicted with the ODT model whereas the data indicates only a single maxima. These differences are attributed to the current implementation of the triplet-mapping events near a wall which will require further research and improvement. Reasonable agreement is observed between the ODT predictions and established inner and outer scaling laws for average temperature and velocity. Comparison of Nusselt number predictions show the correct $Gr_y^{1/3}$ scaling behavior for unity $Pr$ number and $\Pi_t^{1/3}$ scaling for non-unity $Pr$ number cases. A sensitivity study revealed that the results are relatively insensitive to the model constants and all numerical input parameters, highlighting the robustness of this modeling approach.

## Acknowledgements

The work is supported by the Office of Naval Research (ONR) under Grant No. N00014-03-1-0369. The authors are grateful to Dr. Alan Kerstein of Sandia National Laboratories for his extensive discussions and encouragement on the use of ODT for this study.

## References

[1] W.K. George, S.P. Capp, A theory for natural convection turbulent boundary layers next to heated vertical surfaces, J. Heat Mass Transfer 22 (1979) 813–826.
[2] H. Kato, N. Nishiwaki, M. Hirata, On the turbulent heat transfer by free convection from a vertical plate, Int. J. Heat Mass Transfer 11 (1968) 1117–1125.
[3] S. Lin, S.W. Churchill, Turbulent free convection from a vertical, isothermal plate, Numer. Heat Transfer 1 (1978) 129–145.
[4] W.M. To, J.A.C. Humphrey, Numerical simulation of buoyant, turbulent flow – I. free convection along a heated, vertical, flat plate, Int. J. Heat Mass Transfer 29 (1986) 573–592.
[5] J. Salat, S. Xin, P. Joubert, A. Sergent, F. Penot, P. Le Quere, Experimental and numerical investigation of turbulent natural convection in a large air-filled cavity, Int. J Heat Mass Transfer 25 (2004) 824–832.
[6] A.R. Kerstein, One-dimensional turbulence. Model formulation and application to homogeneous turbulence, shear flows, and buoyant statistical flows, J. Fluid Mech. 392 (1999) 277–334.
[7] A.R. Kerstein, One-dimensional turbulence part 2. staircases in double-diffusive convection, Dyn. Atmos. Oceans 30 (1999) 25–46.
[8] A.R. Kerstein, Linear-eddy modeling of turbulent transport. Part 4. Structure of diffusion flames, Combust. Sci. Technol. 81 (1992) 75–96.
[9] T.D. Dreeben, A.R. Kerstein, Simulation of vertical slot convection using 'One-dimensional turbulence', Int. J. Heat Mass Transfer 43 (2000) 3823–3824.
[10] A.R. Kerstein, W.T. Ashurst, S. Wunsch, V. Nilsen, One-dimensional turbulence: vector formulation and application to free shear flows, J. Fluid Mech. 447 (2001) 85–109.
[11] W.T. Ashurst, A.R. Kerstein, L.M. Pickett, J.B. Ghandhi, One-dimensional turbulence: variable-density formulation and application to mixing layers, Phys. Fluids 15 (2003) 579–582.
[12] W.T. Ashurst, A.R. Kerstein, One-dimensional turbulence: variable-density formulation and application to mixing layers, Phys. Fluids 17:025107.
[13] T. Echekki, A.R. Kerstein, D.T. D, J. Chen, 'One-dimensional turbulence' simulations of turbulent jet diffusion flames: model formulation and illustrative applications, Combust. Flame 125 (2001) 1083–1105.
[14] R.C. Schmidt, A.R. Kerstein, S. Wunsch, V. Nilsen, Near-wall LES closure based on one-dimensional turbulence modeling, J. Comput. Phys. 186 (2003) 317–355.
[15] T. Tsuji, Y. Nagano, Velocity and temperature measurements in a natural convection boundary layer along a vertical flat plate, Exp. Thermal Fluid Sci. 2 (1989) 208–215.

[16] T. Wei, One-dimensional turbulence modeling of turbulent wall bounded flows, Ph.D. Thesis, Department of Mechanical Engineering, The University of Utah, Salt Lake City, UT, 2004.
[17] S. Wunsch, A.R. Kerstein, A stochastic model for high Rayleigh number convection, J. Fluid Mech. 528 (2005) 173–205.
[18] S. Ostrach, An analysis of laminar free convection flow and heat transfer about a flat plate parallel to the direction of the generating body force, Tech. Rep. NACA-TN-2635, NACA, 1952.
[19] F.P. Incopera, D.P. DeWitt, Fundamentals of Heat and Mass Transfer, third ed., Wiley, New York, 1990.
[20] E. Ruckenstein, On the laminar and turbulent free convection heat transfer from a vertical plate over the entire range of Prandtl numbers, Int. Commun. Heat Mass Transfer 25 (7) (1998) 1009–1018.
[21] E. Ruckenstein, J. Felske, Turbulent natural convection at high Prandtl numbers, J. Heat Transfer 102 (1980) 773–775.
[22] P. DesJardin, H. Shihn, M.D. Carrara, Combustion SGS modeling for Large Eddy Simulation of fires, in: B. Sunden, M. Faghri (Eds.), Transport Phenomenia of Fires, WIT Press, UK, 2006 (to appear).
[23] A. Papoulis, Probability, Random Variables, and Stochastic Processes, McGraw-Hill, New York, 1991.